FUDMA Journal of Sciences (FJS)
ISSN online: 2616-1370
ISSN print: 2645 - 2944
Vol. 10 No. 24, December, 2026, pp 121 – 132
DOI: https://doi.org/10.33003/fjs-2026-1024-6336

Comparative Mathematical Modelling and Numerical Analysis of Chemotactic Signaling Dynamics in *Escherichia coli*

Zeyad Mohammed Abed

Department of Department of Computer Sciences, College of Sciences, AL-Nahrain University, Jadriya, Baghdad, Iraq.

*Corresponding authors' email: zeyad.mohammed@nahrainuniv.edu.iq

Received: 27 Oct. 2026
Accepted: 09 Nov. 2026
Published: 10 Nov. 2026

ABSTRACT
Chemotaxis enables Escherichia coli to respond to changes in its chemical environment through coordinated receptor activity, intracellular phosphorylation and flagellar motor regulation. Mathematical models provide a quantitative framework for investigating these coupled signalling processes. This study compares the five-equation Clausznitzer chemotaxis model with the four-dimensional Edgington–Tindall reduction and examines the influence of four receptor free-energy formulations on signalling behaviour. The nonlinear ordinary differential equations were integrated in MATLAB with the stiff solver ode15s, and the reduced model was converted to physical time with its published scaling. Responses to a step in attractant concentration were evaluated through receptor activity, adaptation, CheY phosphorylation and predicted flagellar motor bias, and the robustness of the results was tested by tolerance refinement and a one-at-a-time parameter sensitivity analysis. Both models gave an adaptation precision of 1.0000. The adaptation times were 86.4 s for the five-equation model and 165.2 s for the reduced model; with the same Tar-only free energy, the five-equation model adapted in 173.6 s, which indicates that most of the difference arises from receptor composition rather than from model reduction. The three Tar-only free-energy formulations gave adapted-state slopes of −1.000, a value that follows from their mathematical structure, whereas the corresponding experimental value is −0.920 ± 0.003; the mixed-receptor formulation gave −0.423. The predicted motor bias differed markedly between the models because of their different protein totals. Quantitative interpretation therefore requires attention to parameter consistency, time scaling and the limited scope of the experimental benchmarks.

Keywords: *Escherichia Coli Chemotaxis,* Mathematical Modelling, Nonlinear Ordinary Differential Equations, Model Reduction, Receptor Free Energy, Robust Perfect Adaptation, Flagellar Motor, Numerical Simulation

INTRODUCTION

Biological Significance of Chemotaxis

The chemotaxis pathway of *Escherichia coli* is one of the most studied quantitative models of signal transduction in biology (Kargeti et al., 2025). It consists of two modules: a sensing module that transmits environmental signals to the flagellar motors, and an adaptation module that compensates for a constant background stimulus and provides a short-term memory for temporal comparisons (Kargeti et al., 2025). The signalling chain contains a kinase, a response regulator and a phosphatase, which together set the direction of motor rotation and therefore the swimming behaviour of the cell (Bano et al., 2023).

The aspartate receptor Tar and the serine receptor Tsr are the two major chemoreceptors of *E. coli* (Kargeti et al., 2025). Receptor dimers form trimers through contacts between their cytoplasmic tips; two trimers and the kinase CheA form a core signalling complex, and hundreds of core complexes assemble into extended arrays (Koler et al., 2024). Active CheA autophosphorylates its P1 domain, which then donates the phosphoryl group to the response regulator CheY (Koler et al., 2024). Phosphorylated CheY (CheY-P) promotes clockwise (CW) rotation of the flagellar motor (Mattingly & Tu, 2025), and the phosphatase CheZ keeps CheY and CheY-P in a dynamic balance (Bano et al., 2023).

Adaptation is carried out by the methyltransferase CheR, which adds methyl groups to specific glutamyl residues of the receptors, and the methylesterase CheB, which removes them (Kargeti et al., 2025). Each receptor monomer carries four or five modifiable sites (Yue et al., 2023). The methylation state stores the recent activity history of the receptors and therefore allows the cell to detect temporal changes in concentration over a wide range of background levels (Koler et al., 2024). Because the methylation and demethylation rates depend on the kinase output, the adaptation module forms a negative feedback loop (Yue et al., 2023).

Mathematical Models of the Signalling Pathway

Quantitative models of the pathway couple a statistical-mechanical description of ligand binding and receptor methylation with the kinetics of the phosphorylation cascade (Edgington & Tindall, 2018). The receptors act cooperatively: all receptors of a signalling team switch between the active and inactive states together, and the free energy of the team is the sum of the free energies of its dimers (Mandal & Chatterjee, 2022a). The Monod–Wyman–Changeux (MWC) two-state model describes this cooperativity (Mandal & Chatterjee, 2022a). A more general thermodynamic model of trimers of dimers reduces to the MWC model when the coupling energies within and between dimers become very large (Koler et al., 2024).

Clausznitzer et al. (2010) developed a dynamic model of signalling and adaptation from attractant-response experiments, combining cooperative receptor complexes with several layers of feedback regulation. Its whole-pathway form consists of five ordinary differential equations that link the

MWC receptor activity to the phosphorylation of CheA, CheY and CheB, to the CheY-P/CheZ complex and to a methylation feedback (Clausznitzer et al., 2010). Edgington and Tindall (2018) noted that this fifth-order nonlinear system is difficult to treat analytically and analysed a fourth-order reduction, used in earlier work, in which the CheY-P/CheZ complex is neglected. They showed that the reduced system has a single positive steady state, which is asymptotically stable, and proposed that the overshoot observed in experiments can be described as damped oscillations driven by the negative feedback through CheB-P (Edgington & Tindall, 2018).

Robust perfect adaptation is the defining property of this network. Barkai and Leibler (1997) showed that adaptation becomes robust when the modification and demodification rates depend only on the system activity, and that more than 80% of model variants obtained by changing all biochemical parameters randomly by a factor of two still deviated from perfect adaptation by less than 15%. Adaptation is therefore a consequence of the network connectivity rather than of fine-tuned parameters (Barkai & Leibler, 1997). Antoneli et al. (2024) later showed that the reduced Clausznitzer–Edgington–Tindall network shows perfect homeostasis that does not depend on the parameter values.

Receptor Free-Energy Formulations and the Research Gap

In the MWC description, the receptor activity is $A = \frac{1}{1+e^{F}}$, where F is the free-energy difference between the active and inactive states and is composed of a ligand-dependent term and a methylation-dependent term (Yue et al., 2023). Several forms of F have been proposed: a mixed Tar and Tsr form with an average methylation level (Clausznitzer et al., 2010), a Tar-only form (Edgington & Tindall, 2018), a per-dimer form (Mandal & Chatterjee, 2022a) and a log-sensing form (Karin & Alon, 2021). Each form represents a different assumption about how receptor methylation and receptor composition determine the activity of a cluster.

An experimental benchmark for these forms is available. FRET step-response measurements in a Tar-only strain gave a linear relation between the adapted methylation-dependent and ligand-dependent contributions to the free energy, with a slope magnitude of 0.920 ± 0.003, whereas perfect adaptation corresponds to 1.0 (Yue et al., 2023). In the sign convention used in this study, in which the methylation term is plotted against the ligand term, this corresponds to a slope of -0.920 and perfect adaptation to -1. The five-equation model and its four-dimensional reduction, however, differ in receptor composition, parameter values and time scaling. To our knowledge, these effects have not been separated numerically, and the four free-energy forms have not been compared under a single protocol. It therefore remains unclear how much of the difference between the two models is caused by the reduction itself, which properties of the free-energy forms are structural rather than numerical, and how the predicted CheY-P level constrains the motor output of each model.

This study aims to compare the numerical behaviour of established mathematical models of chemotactic signalling in *Escherichia coli* and evaluate the influence of receptor free-energy formulations on adaptation dynamics, intracellular phosphorylation and predicted flagellar motor responses.

MATERIALS AND METHODS

All model equations and parameter values in this section are taken from the cited publications and are used without modification, except for the corrected coefficient in Eq. (17) explained in Section 2.7. The contribution of the present study is the common numerical framework built around these models: identical protocols for both models, conversion of the reduced model to physical time, a simulation that separates the effect of receptor composition from the effect of model reduction, a structural analysis of the adapted-state slope, and convergence and sensitivity analyses.

Overview of the Signaling Cascade

Fig. 1 summarises the network represented by the models. Ligand binding changes the activity A of the receptor complex, which controls the autophosphorylation of CheA. Phosphorylated CheA transfers its phosphoryl group to CheY and CheB, CheY-P is dephosphorylated with the help of CheZ, and CheR and phosphorylated CheB change the average methylation level m of the receptors, which feeds back on A (Clausznitzer et al., 2010; Edgington & Tindall, 2018).

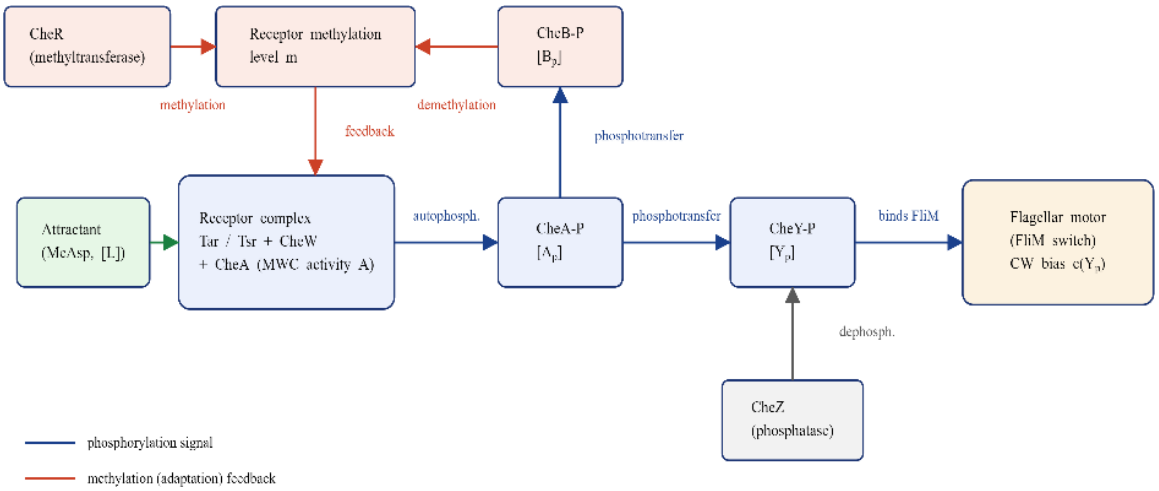


Figure 1: Schematic of the *E. coli* chemotaxis signalling pathway represented by the models. Blue arrows show phosphorylation steps and red arrows show the methylation (adaptation) feedback. The diagram shows the attractant, the receptor complex (Tar/Tsr, CheW and CheA), CheA-P, CheY-P, the phosphatase CheZ, CheB-P, the methyltransferase CheR, the receptor methylation level and the flagellar motor. A, receptor activity; m, average methylation level; $[A_p]$, $[Y_p]$ and $[B_p]$, concentrations of phosphorylated CheA, CheY and CheB

The Clausznitzer Five-Equation Model

The whole-pathway model of Clausznitzer et al. (2010) is written as

$$\frac{d[A_p]}{dt} = Ak_A([A]_{\text{tot}} - [A_p]) - k_Y([Y]_{\text{tot}} - [Y_p])[A_p] - k_B([B]_{\text{tot}} - [B_p])[A_p] \quad (1)$$

$$\frac{d[Y_p]}{dt} = k_Y([Y]_{\text{tot}} - [Y_p])[A_p] - k_1([Z]_{\text{tot}} - [Y_pZ])[Y_p] + k_2[Y_pZ] \quad (2)$$

$$\frac{d[Y_pZ]}{dt} = k_1([Z]_{\text{tot}} - [Y_pZ])[Y_p] - (k_2 + k_3)[Y_pZ] \quad (3)$$

$$\frac{d[B_p]}{dt} = k_B([B]_{\text{tot}} - [B_p])[A_p] - k_{-B}[B_p] \quad (4)$$

$$\frac{\mathrm{dm}}{\mathrm{dt}} = g_R(1 - A) - \hat{g}_B[B_p]^2 A \quad (5)$$

where $[A_p]$, $[Y_p]$, $[Y_pZ]$ and $[B_p]$ (μM) are the concentrations of phosphorylated CheA, free phosphorylated CheY, the CheY-P/CheZ complex and phosphorylated CheB; $[A]_{\text{tot}}$, $[Y]_{\text{tot}}$, $[Z]_{\text{tot}}$ and $[B]_{\text{tot}}$ are the total concentrations; k_A, k_Y, k_B, k_1, k_2, k_3 and k_{-B} are rate constants; m is the average methylation level per receptor; g_R and $\hat{g}_B$ are the effective methylation and demethylation rate constants; and t is time in seconds (Clausznitzer et al., 2010). The conservation terms are those of the original model, and $[Y_p]$ denotes free CheY-P, without the CheY-P/CheZ complex. Eq. (5) is the whole-pathway form of the adaptation kinetics, in which demethylation by CheB-P depends on$[B_p]^2$, with $g_R = 0.006$ s⁻¹ and $\hat{g}_B = 3.14$ μM⁻² s⁻¹ (Clausznitzer et al., 2010, Supporting Text, Table 1). Edgington and Tindall (2018) use the same demethylation term and write the methylation term as$g_R[R_T](1 - \Phi)$. Clausznitzer et al. (2010) also give a simplified form, $g_R(1 - A) - g_B A^3$, with separately fitted constants ($g_R = 0.0069$ s⁻¹ and $g_B = 0.11$ s⁻¹); the constant $\hat{g}_B$ of Eq. (5) applies only to the whole-pathway form and cannot be used in the simplified one. The activity A is given by Eq. (10) with the free energy of Eq. (11). The parameter values are listed in Table 1.

Table 1. Parameters of the Five-Equation Model (Clausznitzer Et Al., 2010)

Symbol	Meaning	Value	Units
$[A]_{\text{tot}}$	Total CheA pool	5.0	μM
$[B]_{\text{tot}}$	Total CheB pool	0.28	μM
$[Y]_{\text{tot}}$	Total CheY pool	9.7	μM
$[Z]_{\text{tot}}$	Total CheZ pool	1.1	μM
k_A	CheA autophosphorylation rate	10	s⁻¹
k_Y	CheY phosphotransfer rate	100	μM⁻¹ s⁻¹
k_B	CheB phosphotransfer rate	15	μM⁻¹ s⁻¹
k_1	CheY-P + CheZ binding	5.0	μM⁻¹ s⁻¹
k_2	$Y_pZ \rightarrow Y_p + Z$	0.5	s⁻¹
k_3	YpZ catalytic	200	s⁻¹
k_{-B}	CheB-P dephosphorylation	1.35	s⁻¹
g_R	Methylation rate constant of Eq. (5)	0.006	s⁻¹
$\hat{g}_B$	Demethylation rate constant of Eq. (5)	3.14	μM⁻² s⁻¹
K_a^{off}	Inactive Tar dissociation	0.02	mM
K_a^{on}	Active Tar dissociation	0.5	mM
K_s^{off}	Inactive Tsr dissociation	100	mM
K_s^{on}	Active Tsr dissociation	10^6	mM
$\nu_a : \nu_s$	Tar : Tsr stoichiometry	1 : 1.4	Dimensionless

The Edgington–Tindall Four-Dimensional Reduction

Edgington and Tindall (2018) neglected the intermediate CheY-P/CheZ complex, rescaled the concentrations by their totals, $[A_p] = a_p[A_T]$, $[Y_p] = y_p[Y_T]$ and $[B_p] = b_p[B_T]$, and rescaled time by the dephosphorylation rate of CheB-P, $t = \tau/k_5$ with $k_5 = 0.7$ s⁻¹. The resulting non-dimensional system is

$$\frac{dm}{d\tau} = \gamma_R(1 - \Phi) - \gamma_B b_p^2 \Phi \quad (6)$$

$$\frac{da_p}{d\tau} = \Phi\bar{k}_1(1 - a_p) - \bar{k}_2(1 - y_p)a_p - \bar{k}_3(1 - b_p)a_p \quad (7)$$

$$\frac{dy_p}{d\tau} = \alpha_1\bar{k}_2(1 - y_p)a_p - (\bar{k}_4 + \bar{k}_6)y_p \quad (8)$$

$$\frac{db_p}{d\tau} = \alpha_2\bar{k}_3(1 - b_p)a_p - \bar{k}_5 b_p \quad (9)$$

where Φ is the receptor activity, and $\bar{k}_1$ to $\bar{k}_6$, α_1, α_2, γ_R and γ_B are dimensionless combinations of the dimensional rate constants and protein totals, for example $\bar{k}_1 = k_1/k_5$, $\gamma_R = g_R[R_T]/k_5$ and $\gamma_B = g_B[B_T]^2/k_5$ (Edgington & Tindall, 2018). Here k_1 tok_6, g_R and g_B are the dimensional constants of Edgington and Tindall (2018) and $[R_T] = 0.16$ μM is the total CheR concentration; their notation differs from that of Eqs. (1) to (5) (for example, their k_5 is the CheB-P dephosphorylation rate, k_{-B} in Eq. (4)). The definitions and values are listed in Table 2. Because$\tau = k_5 t$, any time computed with the reduced model is converted to seconds by dividing by $k_5 = 0.7$ s⁻¹; this conversion is used for all comparisons in Section 3. In Eq. (6) the demethylation term containsb_p^2, in agreement with Eq. (5). Antoneli et al. (2024) showed that the system of Eqs. (6) to (9) shows perfect homeostasis that does not depend on the parameter values.

Table 2: Non-Dimensional Parameters of the Four-Dimensional Reduction (Edgington & Tindall, 2018)

Symbol	Meaning	Definition	Value
$\bar{k}_1$	CheA autophosphorylation	k_1/k_5	48.571
$\bar{k}_2$	CheY phosphotransfer	$k_2[Y_T]/k_5$	1385.714
$\bar{k}_3$	CheB phosphotransfer	$k_3[B_T]/k_5$	6
$\bar{k}_4$	CheY-P dephosphorylation by CheZ	$k_4[Z_T]/k_5$	8.686
$\bar{k}_5$	CheB-P dephosphorylation	k_5/k_5	1
$\bar{k}_6$	CheY-P autodephosphorylation	k_6/k_5	0.121

Symbol	Meaning	Definition	Value
α_1	Concentration ratio	$[A_T]/[Y_T]$	0.814
α_2	Concentration ratio	$[A_T]/[B_T]$	28.214
γ_R	Methylation rate	$g_R[R_T]/k_5$	8.57×10^{-3}
γ_B	Demethylation rate	$g_B[B_T]^2/k_5$	0.352
N	Receptors per signalling team	Not applicable	18
K_a^{off}, K_a^{on}	Tar dissociation constants	Not applicable	0.02 mM, 0.5 mM

Receptor Activity and Free-Energy Formulations

In both models the receptor activity is given by the MWC relation

$$A = \frac{1}{1+e^F} \quad (10)$$

Where$F$, in units ofk_BT, is the free-energy difference between the active and inactive cluster states (Clausznitzer et al., 2010). The four forms of F compared in this study are summarised in Table 3. The mixed Tar and Tsr form of Clausznitzer et al. (2010) is

$$F = N\left[\varepsilon(m) + \nu_a \ln\left(\frac{1+c/K_a^{\text{off}}}{1+c/K_a^{\text{on}}}\right) + \nu_s \ln\left(\frac{1+c/K_s^{\text{off}}}{1+c/K_s^{\text{on}}}\right)\right] \quad (11)$$

Where c is the ligand concentration (written $[L]$ in Eqs. (12) to (14)), $\varepsilon(m) = 1 - 0.5m$, the stoichiometry is $\nu_a{:}\nu_s = 1{:}1.4$, the dissociation constants are $K_a^{\text{off}} = 0.02$ mM, $K_a^{\text{on}} = 0.5$ mM, $K_s^{\text{off}} = 100$ mM and $K_s^{\text{on}} = 10^6$ mM, and the cluster size is $N(c_0) = a_0 + a_1 c_0$ with $a_0 = 17.5$ and $a_1 = 3.35$ mM^{-1} (Clausznitzer et al., 2010). In the present simulations N is evaluated at the baseline concentration $c_0 =$ 0.1 mM. Edgington and Tindall (2018) neglected the low-affinity binding to Tsr, which gives the Tar-only form

$$F = N\left[1 - \frac{m}{2} + \ln\left(\frac{1+[L]/K_a^{\text{off}}}{1+[L]/K_a^{\text{on}}}\right)\right] \quad (12)$$

With $N = 18$ (Edgington & Tindall, 2018). The per-dimer form sums the methylation contribution over the $3n$ dimers of a signalling team (Mandal & Chatterjee, 2022a, 2025; Pramanik et al., 2025):

$$F = 3n \log\left(\frac{1+[L]/K_{\min}}{1+[L]/K_{\max}}\right) + 3n\varepsilon_0 - \sum_j \varepsilon_1 m_j \quad (13)$$

where m_j is the methylation level of dimer j, with $K_{\min} = 18$ μM, $K_{\max} = 3000$ μM and $\varepsilon_0 = \varepsilon_1 = 1\ k_BT$ (Mandal & Chatterjee, 2022a); $n = 6$ is used here so that $3n = 18$, and all dimers are assigned the average methylation level m. The log-sensing form used by Karin and Alon (2021) is

$$F = N[\alpha(1-m) + \ln\frac{1+[L]/K_I}{1+[L]/K_A}] \quad (14)$$

With$\alpha = 1/2$, $K_I = K_a^{\text{off}}$ and $K_A = K_a^{\text{on}}$ in the present calculations. With$\alpha = 1/2$, Eqs. (12) And (14) differ only by the constant$N\alpha$, so their methylation and ligand terms enter in the same way.

Table 3: Free-Energy Formulations Compared in this Study

Form	Equation	Receptors	Methylation Term	Ligand Constants	Source
F_1	(11)	Tar and Tsr (1 : 1.4)	$\varepsilon(m) = 1 - 0.5m$	K_a^{off}, K_a^{on}, K_s^{off}, K_s^{on}	Clausznitzer et al. (2010)
F_2	(12)	Tar only	$1 - m/2$	K_a^{off}, K_a^{on}	Edgington and Tindall (2018)
F_3	(13)	Tar only, per dimer	$\varepsilon_0 - \varepsilon_1 m$ per dimer	$K_{\min}$, $K_{\max}$	Mandal and Chatterjee (2022a)
F_4	(14)	Tar only	$\alpha(1-m)$	K_I, K_A	Karin and Alon (2021)

Coupling to the Flagellar Motor

The CW bias of the motor is related to the CheY-P concentration by a Hill function (Bano et al., 2023)

$$c(y_P) = \frac{y_P^H}{y_P^H + K^H} \quad (15)$$

Where$y_P = [Y_p]$, H is the Hill coefficient and K the half-maximum concentration? Two parameter sets are used (Table 4). Bano et al. (2023) used $H \approx 20$ and $K \approx 3.1$ μM for cells in steady state, taken from earlier work. Mattingly and Tu (2025) reanalysed bead-assay data and obtained $H = 6.0 \pm 0.3$ and $K = 3.24 \pm 0.01$ μM without added Ficoll, while for 19% Ficoll they fixed $H = 10.3$ and $K = 3.1$ μM from the original data source. The higher value of H at the higher viscous load shows that the steepness of the motor response depends on the mechanical conditions (Mattingly & Tu, 2025); this set is not used in the simulations. Eq. (15) gives a predicted switching bias only; it does not describe run lengths, tumbling statistics or cell trajectories. The motor mechanism is not modelled here, although it has been analysed in detail elsewhere (Franco-Oñate et al., 2025; Mattingly & Tu, 2025).

Table 4: Hill-Function Parameters of the Flagellar Motor, Eq. (15)

Parameter Set	H	K (μM)	Measurement Conditions	Use in this Study
Bano et al. (2023)	≈ 20	≈ 3.1	Literature values for cells in steady state, as used by Bano et al.	Main set
Mattingly and Tu (2025)	6.0 ± 0.3	3.24 ± 0.01	Fitted to bead-assay data, 0% Ficoll	Alternative set
Mattingly and Tu (2025)	10.3 (fixed)	3.1 (fixed)	Bead-assay data, 19% Ficoll; values taken from the original data source	Not used (Section 2.5)

Parameter Values

The five-equation model uses the parameters of Clausznitzer et al. (2010) (Table 1), and the reduced model uses the non-dimensional parameters of Edgington and Tindall (2018) (Table 2). The two sets are not identical. The reduced model is based on total concentrations of 7.9 μM CheA, 0.28 μM CheB, 0.16 μM CheR, 9.7 μM CheY and 3.8 μM CheZ, on rate constants of 34 s^{-1} (CheA autophosphorylation), 100 μM^{-1} s^{-1} (CheY phosphotransfer), 15 μM^{-1} s^{-1} (CheB phosphotransfer), 1.6 μM^{-1} s^{-1} (CheY-P dephosphorylation by CheZ), 0.7 s^{-1} (CheB-P dephosphorylation) and 0.085 s^{-1} (CheY-P autodephosphorylation), and on a methylation constant of 0.0375 μM^{-1} s^{-1} and a demethylation constant of 3.14 μM^{-2} s^{-1} (Edgington & Tindall, 2018), whereas the five-

equation model uses 5 μM CheA, 1.1 μM CheZ and different rate constants (Clausznitzer et al., 2010). Clausznitzer et al. (2010) chose their parameters so that the adapted activity is close to 1/3 and the adapted CheY-P concentration is one third of the total CheY. These differences must be taken into account when the outputs of the two models are compared. The effective methylation rate is nevertheless numerically the same in both models: in the reduced model it is $0.0375 \times 0.16 = 0.006$ s^{-1} (equivalently $\gamma_R k_5 = 0.00857 \times 0.7$), which equals $g_R = 0.006$ s^{-1} of the five-equation model.

Numerical Integration

Both systems are stiff; Edgington and Tindall (2018) reported a stiffness ratio of $\lambda_S = 4233.31$ for their parameter set and integrated the model with the MATLAB solver ode15s. The same solver is used here (MATLAB R2025b) with a relative tolerance of 10^{-6} and an absolute tolerance of10^{-9}. The Jacobian is approximated numerically by the solver. The solution is sampled every 0.01 time units (seconds for Eqs. (1) to (5) and τ for Eqs. (6) to (9)), so that event times such as the adaptation time do not depend on the internal step size of the solver.

Each simulation starts with a pre-equilibration at the baseline concentration $c_0 = 100$ μM from the initial state given in Table 5. The final state of this run is the adapted steady state and is used as the initial condition of the step experiment. For the reduced model this state agrees, to within the solver tolerance, with the closed-form steady state of Edgington and Tindall (2018):

$$y_p^* = \frac{\alpha_1 \bar{k}_2 a_p^*}{\alpha_1 \bar{k}_2 a_p^* + \bar{k}_4 + \bar{k}_6} \quad (16)$$

$$b_p^* = \frac{\alpha_2 \bar{k}_3 a_p^*}{\alpha_2 \bar{k}_3 a_p^* + \bar{k}_5} \quad (17)$$

$$\Phi^* = \frac{1}{1 + (\gamma_B/\gamma_R)(b_p^*)^2} \quad (18)$$

$$m^* = 2\left[1 + \ln\left(\frac{1+[L]/K_a^{\mathrm{off}}}{1+[L]/K_a^{\mathrm{on}}}\right) - \frac{1}{N}\ln\left(\frac{\gamma_B (b_p^*)^2}{\gamma_R}\right)\right] \quad (19)$$

Where the asterisk denotes steady-state values. Eqs. (16) to (19) follow from Eqs. (6) to (9) with the time derivatives set to zero. Setting Eq. (9) to zero gives $\bar{k}_3$ in the numerator of Eq. (17); the version printed in Edgington and Tindall (2018, Eq. 16) shows $\bar{k}_2$, which does not satisfy Eq. (9) and does not reproduce the computed steady state, whereas the form of Eq. (17) agrees with it to within the solver tolerance.

Simulation Protocols

The step protocol follows the attractant steps used to fit the original model (Clausznitzer et al., 2010): the concentration of the non-metabolisable attractant α-methyl-aspartate (MeAsp) is raised from 100 μM to 200 μM after the pre-equilibration, and the activity, the phosphorylated protein levels and the methylation level are recorded. The settings of both models are listed in Table 5. In addition, the activity is computed as a function of ligand concentration at fixed methylation levels (input functions), which corresponds to responses faster than adaptation, and the adapted-state relation between the methylation and ligand terms of each free-energy form is computed as described in Section 2.9.

Table 5: Simulation Protocol

Setting	Five-Equation Model	Four-Dimensional Reduction
Initial state of pre-equilibration	$[A_p] = 0.5[A]_{\mathrm{tot}}$, $[Y_p] = 0.5[Y]_{\mathrm{tot}}$, $[Y_pZ] = 0.1[Z]_{\mathrm{tot}}$, $[B_p] = 0.5[B]_{\mathrm{tot}}$, $m = 1$	$a_p = 0.3$, $y_p = 0.3$, $b_p = 0.5$, $m = 1$
Pre-equilibration at 100 μM	2000 s	$\tau = 5000$ (7143 s)
Step 100 → 200 μM MeAsp	$t = 60$ s	$\tau = 200$ (285.7 s)
End of simulation	$t = 600$ s	$\tau = 1500$ (2142.9 s)
Free energy	F_1, Eq. (11) (also F_2, Section 3.2)	F_2, Eq. (12)
Solver and tolerances	ode15s, 10^{-6} / 10^{-9}	ode15s, 10^{-6} / 10^{-9}
Output interval	0.01 s	0.01 τ

Comparison Metrics and Slope Estimation

The adaptation precision is the ratio of the post-step to the pre-step steady-state activity; perfect adaptation corresponds to 1. The peak deviation is the largest absolute difference between the activity and its pre-step value after the step. The adaptation time is the first time after the step at which this difference has fallen to 5% of the peak deviation. The predicted CW bias is obtained by inserting the adapted CheY-P concentration into Eq. (15).

For the input functions, the half-maximum concentration $K_{1/2}$ and an effective Hill exponent n are obtained by a least-squares fit of $A(c) = A_{\min} + \frac{A_{\max} - A_{\min}}{1 + (c/K_{1/2})^n}$ to the activity computed at 400 logarithmically spaced concentrations between 0.01 μM and 10^5 μM. For the adapted-state slope, 40 logarithmically spaced concentrations between 0.1 μM and 10^4 μM are used; at each concentration the methylation level that gives the adapted activity $A^* = 0.34$, the value assumed by Clausznitzer et al. (2010) for their wild-type strain, is found by root finding. The methylation term f_m is then regressed on the ligand term f_L by ordinary least squares. The two terms are the parts of F that depend on m and on the ligand concentration: $f_m = \varepsilon(m)$ and $f_L = \ln\frac{1+c/K_a^{\mathrm{off}}}{1+c/K_a^{\mathrm{on}}}$ for F_1; $f_m = 1 - m/2$ and the same f_L for F_2; $f_m = 1 - m$ and $f_L = \ln\frac{1+[L]/K_{\min}}{1+[L]/K_{\max}}$ for F_3; and $f_m = \alpha(1-m)$ with the same f_L as F_2 for F_4. The standard error of the slope and the coefficient of determination are reported. This follows the representation of Yue et al. (2023), with the sign convention stated in Section 1.3. For F_2 to F_4 the slope does not depend on the chosen A^* (Section 3.4).

Convergence and Sensitivity Analysis

Numerical convergence is tested by repeating the step simulations with tolerance pairs of $10^{-8}/10^{-11}$ and $10^{-10}/10^{-13}$, comparing both the summary metrics and the maximum absolute difference of the activity and CheY-P trajectories from the solution with the tightest tolerances. Parameter sensitivity is tested one parameter at a time: each rate constant of Eqs. (1) to (5) and each dimensionless parameter of Eqs. (6) to (9), including the concentration ratios α_1 and α_2, is multiplied by 0.5, 0.9, 1.1 and 1.5 while all other parameters are kept at their reference values, giving 76 simulations, and the adaptation precision, the adapted activity, the peak deviation and the adaptation time are recorded. The protein totals of the five-equation model are not varied separately.

Implementation and Reproducibility

The MATLAB code that produces all numerical results, tables and figures is provided as supplementary material, together with a README file that lists each script, the order in which they are run and the output files. The parameter values, initial conditions, tolerances and protocol settings are defined in the code and in Tables 1, 2, 4 and 5.

RESULTS AND DISCUSSION

Step Responses of the Two Models on a Common Time Scale

Fig. 2 shows the step response of the five-equation model. Before the step, the adapted activity is $A^* = 0.333$ and the adapted CheY-P concentration is 3.25 µM, close to the values of 1/3 and $[Y]_{\mathrm{tot}}/3 = 3.23$ µM for which the model was parameterised (Clausznitzer et al., 2010). When the attractant concentration is doubled, the activity falls at once by 0.316, that is 95% of its adapted value, and CheY-P falls to 0.165 µM. The methylation level then rises from 3.264 to 3.642, and the activity returns to its pre-step value with an adaptation time of 86.4 s and a precision of 1.0000.

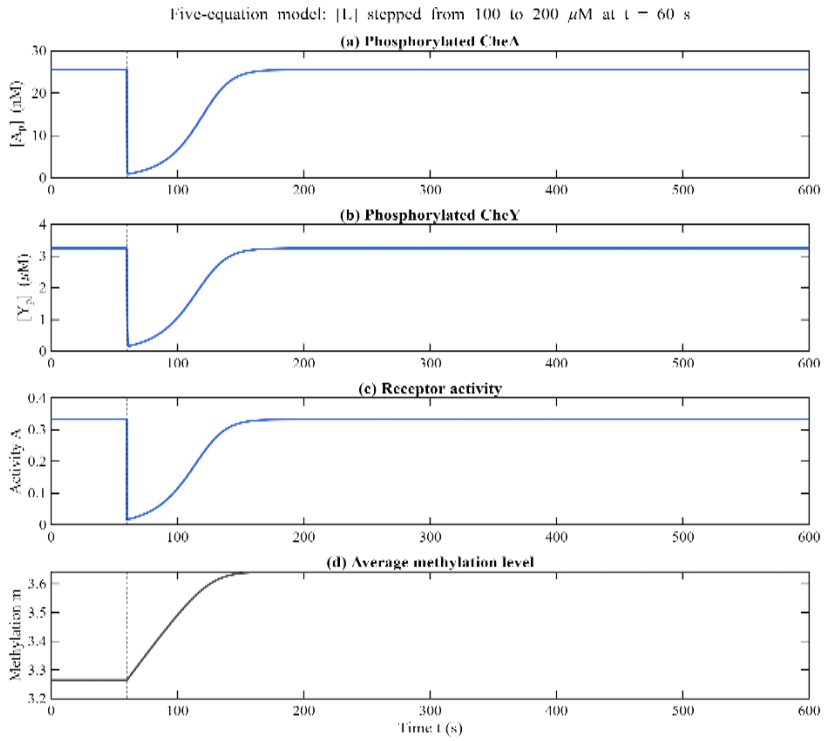


Figure 2: Step response of the five-equation model, Eqs. (1) to (5) withF_1. The MeAsp concentration is raised from 100 to 200 µM at $t = 60$ s (dashed line). (a) Phosphorylated CheA; (b) phosphorylated CheY; (c) receptor activity$A$; (d) average methylation level$m$. Time is in seconds

Figure 3 shows the same protocol for the four-dimensional reduction. The adapted activity is $\Phi^* = 0.094$, the activity falls almost to zero after the step (100% of Φ^*), and it recovers after 115.7 non-dimensional time units. With $t = \tau/k_5$ this corresponds to 165.2 s. The methylation level rises from 4.967 to 5.871, and the precision is again 1.0000. The recovery is monotonic, which is consistent with the asymptotically stable steady state reported by Edgington and Tindall (2018).

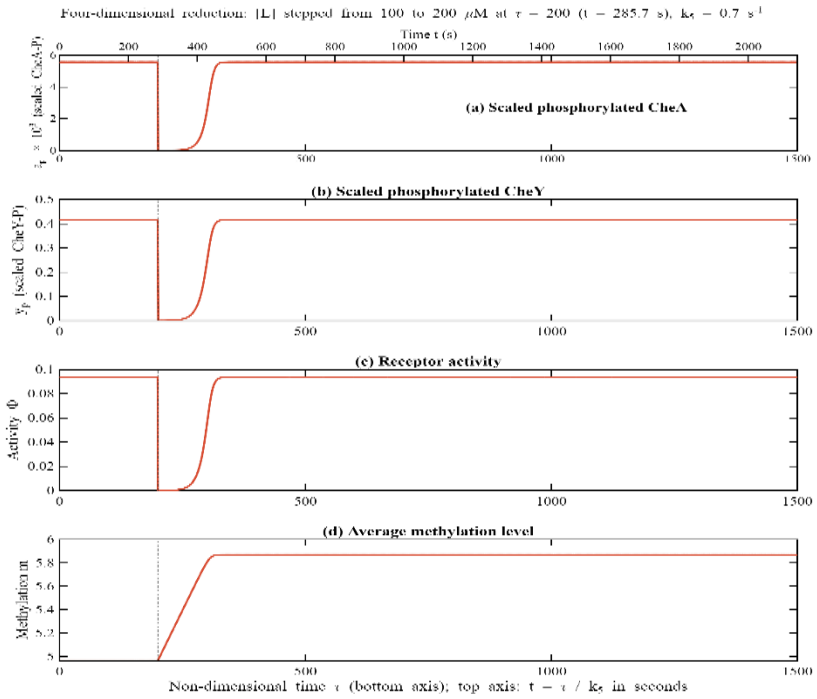


Figure 3: Step response of the four-dimensional reduction, Eqs. (6) to (9). The bottom axes show the non-dimensional time τ and the top axis of panel (a) shows the corresponding time $t = \tau/k_5$ in seconds ($k_5 = 0.7$ s^{-1}). The MeAsp concentration is raised from 100 to 200 μM at $\tau = 200$ (dashed line). (a) Scaled phosphorylated CheA a_p (multiplied by10^3); (b) scaled phosphorylated CheYy_p; (c) receptor activityΦ; (d) average methylation level m

On a common time scale (Fig. 4), the reduced model adapts about twice as slowly as the five-equation model (165.2 s against 86.4 s). Its adapted activity is lower (0.094 against 0.333) and its adapted CheY-P concentration is higher (4.04 μM against 3.25 μM), because the two models use different protein totals and rate constants (Section 2.6). In both models the peak of the response occurs at the moment of the step, because Eq. (10) assumes that the receptor cluster switches instantly between its two states; Mandal and Chatterjee (2022b) showed that a finite switching time scale of receptor activity changes chemotactic performance, so the instantaneous drop is a property of the model assumption rather than a prediction.

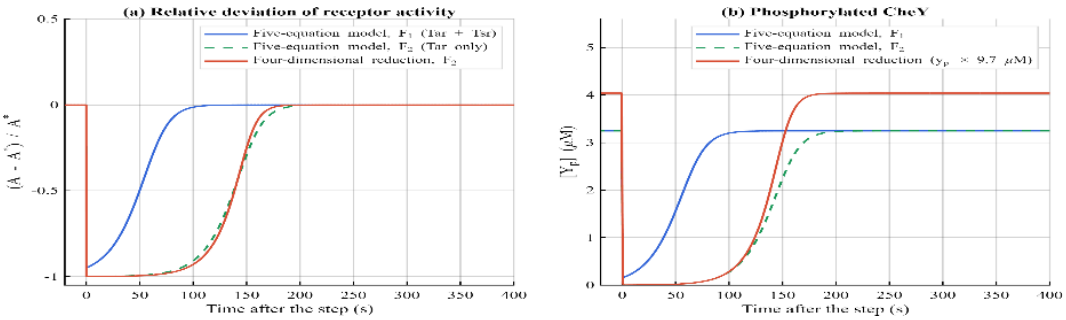


Figure 4: Comparison of the models on a common time scale (seconds after the step). (a) Relative deviation of the activity from its adapted value; (b) CheY-P concentration, with y_p of the reduced model converted to μM by $[Y_T] = 9.7$ μM. Blue: five-equation model withF_1; dashed green: five-equation model withF_2; red: four-dimensional reduction withF_2

Effect of Model Reduction versus Receptor Composition

The two models differ in two respects at the same time: the reduction removes the CheY-P/CheZ complex and changes the parameter set, and the free energy changes from the mixed form F_1 to the Tar-only formF_2. To separate these effects, the five-equation model was run with F_2 (with$N = 18$, as in the reduced model) instead of F_1 (dashed green line in Fig. 4). Its adaptation time increased from 86.4 s to 173.6 s, about 5% longer than the 165.2 s of the reduced model. The relative peak deviation also became almost identical to that of the reduced model (99.96% against 99.97%). The adapted activity did not change (0.333), because at steady state Eq. (5) fixes the activity independently of the form of$F$.

Most of the difference in adaptation time between the two models is therefore caused by the receptor composition of the free energy and not by the reduction itself. In F_1 the Tar term is weighted by$\nu_a = 1/2.4$, so a given change in ligand concentration changes F less and requires a smaller change in methylation; this explains the faster adaptation of the mixed form. Consistently, the methylation level changes by 0.378

after the step with F_1 and by 0.904 in the reduced model, a ratio of 2.39, close to $1/\nu_a = 2.4$. The remaining difference of about 5% reflects the reduction and the different parameter sets. The methylation rate is the same in both models (Section 2.6), which is consistent with their adaptation times becoming comparable once the free energy is the same. This single substitution suggests that the reduced model captures the adaptation time scale of the full model when the receptor composition is matched; it does not show that the two models are quantitatively equivalent, and the reduced model does not reproduce the absolute activity and CheY-P levels of the full model (Fig. 4b), which depend on the different parameter sets.

Activity Input Functions and Free-Energy Formulations

Fig. 5 shows the activity as a function of ligand concentration at four fixed methylation levels for F_1 andF_2. At each methylation level the activity is a decreasing sigmoid ofln$[L]$, and a higher methylation level shifts the curve to higher concentrations, as expected from the methylation term of Eqs. (11) and (12). These curves represent responses faster than adaptation, which is the situation probed by FRET dose-response measurements (Clausznitzer et al., 2010); the comparison with those measurements is qualitative only.

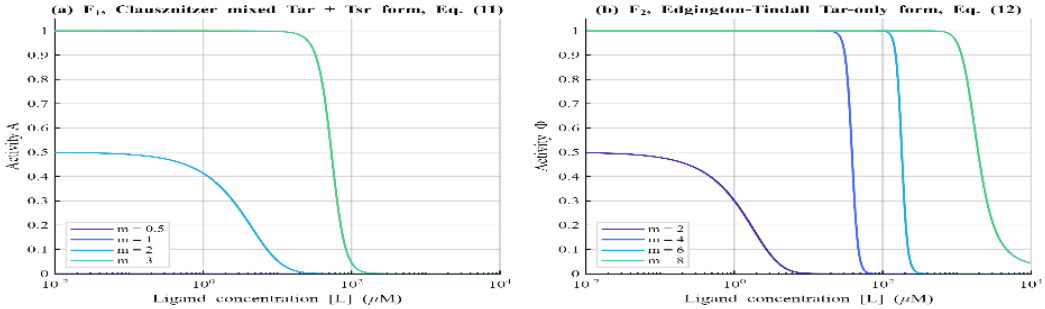


Figure 5: Activity input functions at fixed methylation levels. (a) F_1, mixed Tar and Tsr form, Eq. (11), with the parameters of Table 1; (b) F_2, Tar-only form, Eq. (12), with the parameters of Table 2. Each curve is the activity at the indicated constant methylation level m as a function of the ligand concentration $[L]$

Fig. 6 compares the four forms at$m = 3$. The fitted half-maximum concentrations are 53.2 μM forF_1, 13.8 μM forF_2, 120.3 μM for F_3 and 38.5 μM forF_4, with effective Hill exponents of 4.6, 6.8, 15.0 and 10.5, respectively. All four forms use a multiplier of about 18 for the ligand term, so the steepness of F_3 comes from its ligand constants: the ratio $K_{\max}/K_{\min} = 3000/18 \approx 167$ (Mandal & Chatterjee, 2022a) is much larger than the ratio $K_a^{\mathrm{on}}/K_a^{\mathrm{off}} = 25$ of the Tar constants, so the ligand term changes F over a wider range. The differences in half-maximum concentration therefore reflect the different dissociation constants and methylation offsets of the forms, not a better or worse description of the same data.

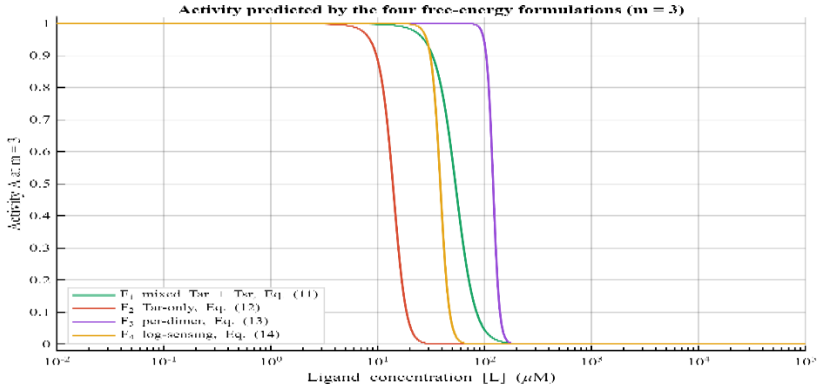


Figure 6: Activity predicted by the four free-energy formulations at the methylation level $m = 3$: F_1, Eq. (11); F_2, Eq. (12); F_3, Eq. (13); F_4, Eq. (14). All forms use the activity relation of Eq. (10)

Adapted-State Slope: Structural Origin and Experimental Comparison

Fig. 7 shows the adapted-state relation between the methylation term f_m and the ligand termf_L. The slopes are −1.000 forF_2, F_3 andF_4, with standard errors below 10^{-15} and$R^2 = 1$, and −0.423 ± 0.001 for F_1 ($R^2 = 0.9997$).

The value of −1 is not a numerical finding but a direct consequence of the structure of the three Tar-only forms. At the adapted state the activity is constant, so F is constant. In Eqs. (12) to (14) the methylation and ligand terms enter the free energy additively and with the same weight, so a constant F implies $f_m = -f_L + const$, that is, a slope of exactly −1, whatever the values of the parameters. In Eq. (11) the Tar term is multiplied by ν_a, so the same argument gives a slope of $-\nu_a = -1/2.4 \approx -0.417$ when the Tsr term is negligible. The computed value of −0.423 differs from −0.417 by about 1.5% because the Tsr term is small but not zero over the concentration range used. The same argument shows that the slopes of F_2 to F_4 do not depend on the adapted activity chosen for the calculation.

Yue et al. (2023) measured a slope of 0.920 ± 0.003 in magnitude in a Tar-only strain, which is −0.920 in the convention used here (Section 1.3). The difference between −1.000 and −0.920 is much larger than the experimental

uncertainty, so the Tar-only forms do not reproduce this measurement quantitatively. Yue et al. (2023) attributed the imprecise adaptation to the distribution of CheR along the modifiable sites that results from the tethered motion of the enzyme, a mechanism that is not part of any of the four forms. The value of −0.423 obtained with F_1 cannot be compared with this measurement either, because F_1 describes a cell with both Tar and Tsr, whereas the experiment used a Tar-only strain. The slope analysis therefore shows how the receptor composition assumed in each form determines the adapted-state relation, but it does not establish that one form describes the data better than another.

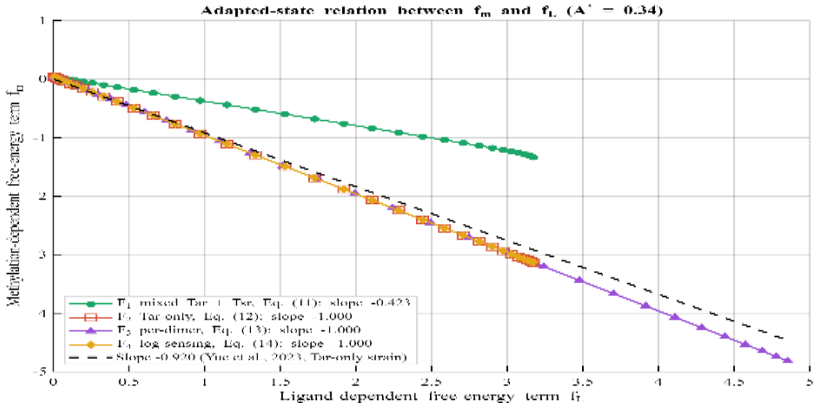


Figure 7: Adapted-state relation between the methylation-dependent term f_m and the ligand-dependent term f_L of the free energy for the four formulations, at $A^* = 0.34$. The slope of each line is given in the legend. The open squares of F_2 coincide with the diamonds of F_4. The dashed line has the slope −0.920, which corresponds to the slope magnitude of 0.920 measured by Yue et al. (2023) in a Tar-only strain

Predicted Flagellar Motor Bias

Fig. 8 shows the two Hill functions of Table 4 together with the adapted CheY-P concentrations of the two models. With the parameters of Bano et al. (2023), the 10% to 90% range of the CW bias spans only 0.68 µM of CheY-P (2.78 to 3.46 µM), compared with 2.43 µM (2.25 to 4.67 µM) for the parameters of Mattingly and Tu (2025). At the adapted CheY-P level of the five-equation model (3.25 µM), the predicted CW bias is 0.72 with the first set and 0.50 with the second; at the level of the reduced model (4.04 µM), it is 0.995 and 0.79. These values show that the steep motor function amplifies the difference in CheY-P between the two models into a large difference in predicted motor output. Bano et al. (2023) reported a mean CW bias of 0.12 in free-swimming cells. Inverting Eq. (15) shows that this value would require an adapted CheY-P concentration of about 2.8 µM with the parameters of Bano et al. (2023) or 2.3 µM with those of Mattingly and Tu (2025), which is lower than the adapted level of either model. This indicates that the adapted CheY-P levels of the two parameter sets and the motor parameters are not mutually consistent, so a common calibration would be needed before motor output is compared with behavioural data. This comparison concerns the predicted switching bias only; Eq. (15) does not predict run lengths, tumbling frequencies or swimming trajectories, and the Hill parameters were obtained under different mechanical conditions (Mattingly & Tu, 2025).

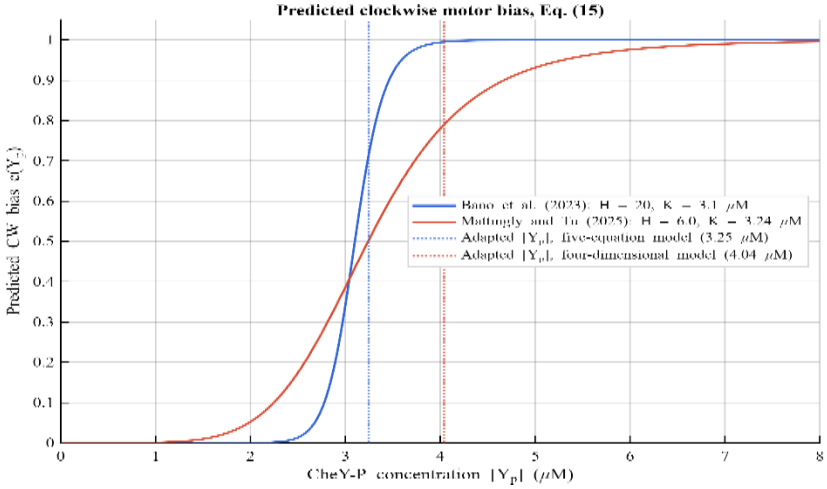


Figure 8: Predicted clockwise motor bias as a function of the CheY-P concentration, Eq. (15), for the parameter sets of Bano et al. (2023), $H = 20$ and $K = 3.1$ µM, and Mattingly and Tu (2025), $H = 6.0$ and $K = 3.24$ µM. The dotted lines mark the adapted CheY-P concentrations of the five-equation model and of the four-dimensional reduction

Numerical Convergence and Parameter Sensitivity

Table 6 shows that all summary metrics agree to at least seven significant digits for the three tolerance pairs. Because several of these metrics are steady-state values or are read on the fixed output grid, the whole trajectories were also compared: with the reference tolerances, the activity differs from the tightest-tolerance solution by at most 5.4×10^{-7} and the CheY-P concentration by at most 6.4×10^{-6} µM over the entire simulation. The results are therefore not affected by the solver tolerances.

Table 6: Convergence Test: Step-Response Metrics for Three Tolerance Pairs

RelTol / AbsTol	Model	Precision	A^*	Peak deviation	Adaptation time (s)	$[Y_p]^*$ (µM)
10^{-6} / 10^{-9}	Five-equation	1.000000	0.332912	0.316026	86.36	3.2465
10^{-6} / 10^{-9}	Four-dimensional	1.000000	0.093647	0.093617	165.24	4.0398
10^{-8} / 10^{-11}	Five-equation	1.000000	0.332912	0.316026	86.36	3.2465
10^{-8} / 10^{-11}	Four-dimensional	1.000000	0.093647	0.093617	165.24	4.0398
10^{-10} / 10^{-13}	Five-equation	1.000000	0.332912	0.316026	86.36	3.2465
10^{-10} / 10^{-13}	Four-dimensional	1.000000	0.093647	0.093617	165.24	4.0398

The sensitivity analysis (Table 7 and Fig. 9) shows that the adaptation precision remained 1.0000 in all 76 simulations. This agrees with the parameter-independent perfect adaptation established for this class of networks (Barkai & Leibler, 1997; Antoneli et al., 2024) and is a numerical check of that property, not a new result. The adaptation time is controlled mainly by the methylation rate: halving g_R or γ_R increased the adaptation time by 94% and 99%, and increasing g_R or γ_R by 50% reduced it by 32% and 33%. All other parameters changed the adaptation time by at most 17% in the five-equation model and 3% in the reduced model, although several of them changed the adapted activity (Table 7).

Table 7: One-At-A-Time Sensitivity of the Adaptation Time (Relative Change In %) and of the Adapted Activity. The Adaptation Precision was 1.0000 in all Cases

Model	Parameter	× 0.5	× 0.9	× 1.1	× 1.5	A^* at × 0.5 / × 1.5
Five-equation	k_A	+16.5	+1.8	−1.5	−5.6	0.496 / 0.258
Five-equation	k_Y	−2.5	−0.5	+0.4	+2.1	0.249 / 0.388
Five-equation	k_B	+4.2	+0.5	−0.4	−1.7	0.431 / 0.282
Five-equation	k_1	−8.6	−1.2	+1.0	+3.8	0.275 / 0.356
Five-equation	k_2	0.0	0.0	0.0	0.0	0.333 / 0.333
Five-equation	k_3	−1.3	−0.1	+0.1	+0.4	0.327 / 0.335
Five-equation	k_{-B}	−3.4	−0.6	+0.6	+2.6	0.248 / 0.389
Five-equation	g_R	+94.3	+10.6	−8.7	−32.0	0.277 / 0.369
Five-equation	$\hat{g}_B$	+4.3	+0.6	−0.5	−2.1	0.396 / 0.299
Four-dimensional	$\bar{k}_1$	+0.9	+0.1	−0.1	−0.2	0.143 / 0.073
Four-dimensional	$\bar{k}_2$	+1.8	+0.3	−0.2	−1.0	0.073 / 0.108
Four-dimensional	$\bar{k}_3$	−1.6	−0.2	+0.2	+1.0	0.119 / 0.081
Four-dimensional	$\bar{k}_4$	−2.8	−0.4	+0.3	+1.2	0.074 / 0.102
Four-dimensional	$\bar{k}_5$	+1.1	+0.2	−0.2	−0.7	0.072 / 0.108
Four-dimensional	$\bar{k}_6$	0.0	0.0	0.0	0.0	0.093 / 0.094
Four-dimensional	α_1	+1.8	+0.3	−0.3	−1.5	0.107 / 0.083
Four-dimensional	α_2	−1.6	−0.2	+0.2	+1.0	0.119 / 0.081
Four-dimensional	γ_R	+99.3	+11.1	−9.0	−33.2	0.074 / 0.108
Four-dimensional	γ_B	+1.0	+0.1	−0.1	−0.5	0.120 / 0.081

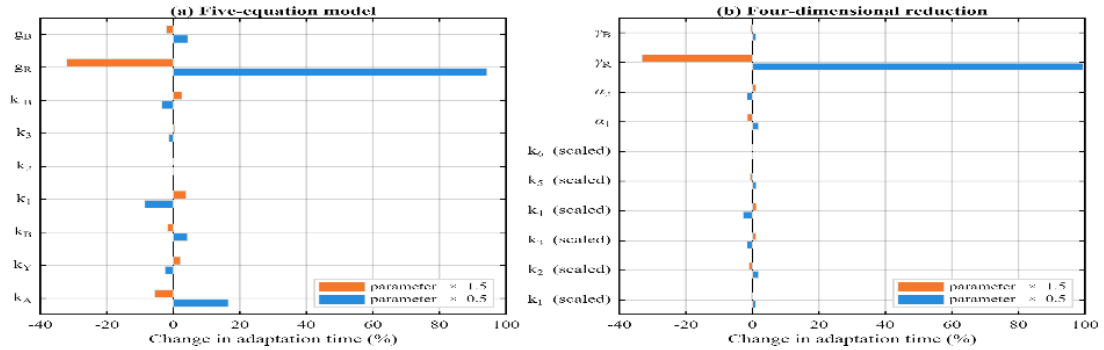


Figure 9: Relative change in the adaptation time when each model parameter is multiplied by 0.5 (blue) or 1.5 (orange). (a) Five-equation model, Eqs. (1) to (5); (b) four-dimensional reduction, Eqs. (6) to (9)

Summary of Comparison Metrics

Table 8 summarises the metrics and states, for each comparison with published values, whether it is a direct quantitative comparison, a consistency check with the original parameterisation, a reproduction of an established theoretical property or only a qualitative comparison.

Table 8: Summary of Comparison Metrics

Metric	Five-equation, F_1	Five-equation, F_2	Four-dimensional, F_2	Published value	Type of comparison
Adaptation precision	1.0000	1.0000	1.0000	1 (Barkai & Leibler, 1997; Antoneli et al., 2024)	Reproduction of an established property
Adapted activity A^*	0.333	0.333	0.094	$\approx$ 1/3 (Clausznitzer et al., 2010)	Consistency with the parameterisation (five-equation model)
Adapted $[Y_p]$ (μM)	3.25	3.25	4.04	$[Y]_{\mathrm{tot}}/3 = 3.23$ (Clausznitzer et al., 2010)	Consistency with the parameterisation (five-equation model)
Peak deviation / A^*	0.949	1.000	1.000	Not available	Model output
Adaptation time (s)	86.4	173.6	165.2	$\tau_2 = 9.9 \pm 0.3$ s, impulse response (Mattingly et al., 2021)	Not directly comparable (different protocol)
Predicted CW bias (Bano / Mattingly–Tu)	0.72 / 0.50	Same as F_1	0.995 / 0.79	0.12, free-swimming cells (Bano et al., 2023)	Qualitative only
Adapted f_m versus f_L slope	−0.423	−1.000	−1.000	−0.920 ± 0.003 in the convention used here, Tar-only strain (Yue et al., 2023)	Direct for the Tar-only forms (not reproduced); not comparable for F_1 (Section 3.4)

The adaptation times cannot be compared directly with the slow time constant $\tau_2 = 9.9 \pm 0.3$ s of the kinase response kernel (Mattingly et al., 2021), because that kernel was obtained from small concentration changes around a background, whereas a doubling of the attractant concentration drives the methylation level through a large change.

Contribution, Relation to Previous Work and Limitations

The models, parameter values and free-energy forms used here are taken from the literature, and perfect adaptation is a known property of these networks (Barkai & Leibler, 1997; Antoneli et al., 2024). The contribution of this study is a reproducible comparative framework that (i) places the full and reduced models on a common physical time scale, (ii) shows that the difference in adaptation time between them is caused mainly by receptor composition rather than by the reduction, (iii) explains the slope of −1 of the Tar-only forms as a structural property and the slope of the mixed form as a consequence of the Tar fraction, (iv) quantifies how the motor Hill function relates the adapted CheY-P level to the predicted motor bias, and (v) checks the published equations and parameter values used in the simulations, including the steady-state expression of Eq. (17).

The results relate to several recent studies. The long adaptation times obtained here reflect the slow methylation dynamics, which Mayo and Soto (2025) linked to a nonlocal response with time and length scales of about 19 s and 170 μm that can make the Keller–Segel equations invalid on these scales. Chatterjee (2022) derived an exact condition for the extremal response of the activity after a step and predicted an optimal step size at which the extremal response is reached in the shortest time, which is a complementary view of the transient phase studied here. The per-dimer form F_3 is the basis of the stochastic simulations of Mandal and Chatterjee (2022a, 2025) and Pramanik et al. (2025), and the log-sensing form F_4 underlies the analysis of temporal gain fluctuations by Karin and Alon (2021). Moore et al. (2023) showed that the distribution of single-cell sensitivities to attractants in mixed backgrounds is tuned at the population level, which a single deterministic model cannot represent.

Several limitations apply. First, both models are deterministic, whereas Mattingly et al. (2024) described the kinase activity of single cells as a noisy process with a correlation time of 8.7 ± 0.9 s (measured at a background of 1 μM aspartate), and Mattingly et al. (2021) showed that chemotactic performance is limited by the rate at which the cell acquires information through its signalling pathway. Second, the cluster size is constant or a smooth function of the background concentration, and the receptor switching is instantaneous, although a finite switching rate affects chemotactic performance (Mandal & Chatterjee, 2022b). Third, the two models use different parameter sets, so differences in absolute activity and CheY-P levels reflect the parameterisation as much as the model structure, and the protein totals were not varied in the sensitivity analysis. Fourth, the steepness of the motor response depends on the mechanical load (Mattingly & Tu, 2025), and Eq. (15) predicts only the switching bias. Finally, the comparison with published benchmarks is limited to a few selected quantities; agreement with these values, where it occurs, does not constitute a comprehensive experimental validation of either model.

Conclusion

This study compared the numerical behaviour of the Clausznitzer five-equation chemotaxis model and the four-dimensional Edgington–Tindall reduction to investigate receptor adaptation, intracellular signalling and predicted flagellar motor responses in *Escherichia coli*. Both models reproduced perfect adaptation under the simulated conditions, with an adaptation precision of 1.0000 that was unaffected by the solver tolerances and by one-at-a-time parameter changes of up to 50%. After conversion to physical time, the adaptation times were 86.4 s and 165.2 s; when the five-equation model was given the same Tar-only free energy, its adaptation time became 173.6 s, which indicates that receptor composition rather than model reduction causes most of this difference. The three Tar-only free-energy formulations produced adapted-state slopes of −1.000 as a direct consequence of their structure, whereas the mixed-receptor formulation yielded −0.423; none of them reproduced the experimental value of −0.920 ± 0.003. The Hill-function analysis showed that the predicted motor bias is highly sensitive to the adapted CheY-P level and to the selected motor parameters. The findings provide a computational basis for comparing established chemotaxis models, but their interpretation remains limited by the deterministic assumptions, the differences between the parameter sets and the reliance on a few published experimental benchmarks. Future investigations should include stochastic signalling effects, a common parameterisation of both models and

further validation against independent experimental measurements.

REFERENCES

Antoneli, F., Golubitsky, M., Jin, J., & Stewart, I. (2024). *Homeostasis in input-output networks: Structure, classification and applications* [Preprint]. arXiv. https://doi.org/10.48550/arXiv.2405.03861

Bano, R., Mears, P., Golding, I., & Chemla, Y. R. (2023). Flagellar dynamics reveal fluctuations and kinetic limit in the *Escherichia coli* chemotaxis network. *Scientific Reports, 13*, Article 22891. https://doi.org/10.1038/s41598-023-49784-w

Barkai, N., & Leibler, S. (1997). Robustness in simple biochemical networks. *Nature, 387*(6636), 913–917. https://doi.org/10.1038/43199

Chatterjee, S. (2022). Short time extremal response to step stimulus for a single cell *E. coli*. *Journal of Statistical Mechanics: Theory and Experiment, 2022*(12), Article 123503. https://doi.org/10.1088/1742-5468/aca589

Clausznitzer, D., Oleksiuk, O., Løvdok, L., Sourjik, V., & Endres, R. G. (2010). Chemotactic response and adaptation dynamics in *Escherichia coli*. *PLOS Computational Biology, 6*(5), Article e1000784. https://doi.org/10.1371/journal.pcbi.1000784

Edgington, M. P., & Tindall, M. J. (2018). Mathematical analysis of the *Escherichia coli* chemotaxis signalling pathway. *Bulletin of Mathematical Biology, 80*(4), 758–787. https://doi.org/10.1007/s11538-018-0400-z

Franco-Oñate, M.-J., Parmeggiani, A., Dorignac, J., Geniet, F., Walter, J.-C., Pedaci, F., Nord, A. L., Palmeri, J., & Walliser, N.-O. (2025). Signature of cooperativity in the stochastic fluctuations of small systems with application to the bacterial flagellar motor. *Scientific Reports, 15*, Article 32109. https://doi.org/10.1038/s41598-025-14570-3

Kargeti, M., Kalita, I., Hoch, S., Ratnikava, M., Xu, W., Ni, B., Dy, R. L., Colin, R., & Sourjik, V. (2025). Experimental evolution partially restores functionality of bacterial chemotaxis network with reduced number of components. *PLOS Genetics, 21*(7), Article e1011784. https://doi.org/10.1371/journal.pgen.1011784

Karin, O., & Alon, U. (2021). Temporal fluctuations in chemotaxis gain implement a simulated-tempering strategy for efficient navigation in complex environments. *iScience, 24*(7), Article 102796. https://doi.org/10.1016/j.isci.2021.102796

Koler, M., Parkinson, J. S., & Vaknin, A. (2024). Signal integration in chemoreceptor complexes. *Proceedings of the National Academy of Sciences of the United States of America, 121*(14), Article e2312064121. https://doi.org/10.1073/pnas.2312064121

Mandal, S. D., & Chatterjee, S. (2022a). Effect of receptor cooperativity on methylation dynamics in bacterial chemotaxis with weak and strong gradient. *Physical Review E, 105*(1), Article 014411. https://doi.org/10.1103/PhysRevE.105.014411

Mandal, S. D., & Chatterjee, S. (2022b). Effect of switching time scale of receptor activity on chemotactic performance of *Escherichia coli*. *Indian Journal of Physics, 96*(9), 2619–2627. https://doi.org/10.1007/s12648-021-02259-y

Mandal, S. D., & Chatterjee, S. (2025). Bacterial chemotaxis in a traveling wave attractant environment. *Journal of Statistical Mechanics: Theory and Experiment, 2025*(6), Article 063501. https://doi.org/10.1088/1742-5468/add868

Mattingly, H. H., Kamino, K., Machta, B. B., & Emonet, T. (2021). *Escherichia coli* chemotaxis is information limited. *Nature Physics, 17*(12), 1426–1431. https://doi.org/10.1038/s41567-021-01380-3

Mattingly, H. H., Kamino, K., Ong, J., Kottou, R., Emonet, T., & Machta, B. B. (2024). *Chemotaxing E. coli do not count single molecules* [Preprint]. arXiv. https://doi.org/10.48550/arXiv.2407.07264

Mattingly, H. H., & Tu, Y. (2025). *Ultrasensitivity without conformational spread: A mechanical origin for non-equilibrium cooperativity in the bacterial flagellar motor* [Preprint]. arXiv. https://doi.org/10.48550/arXiv.2502.03290

Mayo, M., & Soto, R. (2025). *Bacterial chemotaxis considering memory effects* [Preprint]. arXiv. https://doi.org/10.48550/arXiv.2504.15385

Moore, J. P., Kamino, K., Kottou, R., Shimizu, T. S., & Emonet, T. (2023). *Signal integration and adaptive sensory diversity tuning in Escherichia coli chemotaxis* [Preprint]. bioRxiv. https://doi.org/10.1101/2023.02.08.527720

Pramanik, R., Yadav, R. K., & Chatterjee, S. (2025). Dynamics of chemoreceptor activity with time-periodic attractant field. *The European Physical Journal E, 48*, Article 60. https://doi.org/10.1140/epje/s10189-025-00525-z

Yue, C., Zhang, C., Zhang, R., & Yuan, J. (2023). Tethered particle motion of the adaptation enzyme CheR in bacterial chemotaxis. *iScience, 26*(10), Article 107950. https://doi.org/10.1016/j.isci.2023.107950

©2026 This is an Open Access article distributed under the terms of the Creative Commons Attribution 4.0 International license viewed via https://creativecommons.org/licenses/by/4.0/ which permits unrestricted use, distribution, and reproduction in any medium, provided the original work is cited appropriately.